

System-level thermal and electrical modeling of battery systems for electric aircraft design

Thomas Kuijpers, Jorn van Kampen and Theo Hofman

August 30, 2024

Abstract—This work introduces a framework for simulating the electrical power consumption of an 8-seater electric aircraft equipped with high-energy-density NMC Lithium-ion cells. We propose an equivalent circuit model (ECM) to capture the thermal and electrical battery behavior. Furthermore, we assess the need for a battery thermal management system (BTMS) by determining heat generation at the cell level and optimize BTMS design to minimize energy consumption over a predefined flight regime. The proposed baseline battery design includes a 304-kWh battery system with BTMS, ensuring failure redundancy through two parallel switched battery banks. Simulation results explore the theoretical flight range without BTMS and reveal advantages in increasing battery capacity under specific conditions. Optimization efforts focus on BTMS design, highlighting the superior performance of water cooling over air cooling. However, the addition of a 9.9 kW water-cooled BTMS results in a 16.5% weight increase (387 kg) compared to no BTMS, reducing the simulated range of the aircraft from 480 km to 410 km. Lastly, we address a heating-induced thermal runaway scenario, demonstrating the robustness of the proposed battery design in preventing thermal runaway.

I. INTRODUCTION

Electric aviation, driven by emission reduction goals like EU ACARE Flightpath 2050 and NASA's N+3 program, has promising potential to lower the aviation industry's carbon footprint [1]. However, current technological limitations restrict large electric passenger aircraft to light and short-distance flights [2]. To address this, companies are exploring small-scale, short-distance passenger aircraft using advanced High Energy Density (HED) Lithium-ion battery (LIB) technology. LIBs of the 'pouch' type are preferred for their efficient packing and capacity [3]. Increasing battery capacity extends flight range but adds weight, affecting energy consumption and design optimization. Safety concerns, especially maintaining optimal battery temperature, are critical [4]. A battery thermal management system (BTMS) is essential for safety and efficiency. This study proposes a minimum-energy framework to manage heat generation in a pouch-type battery system for an 8-seater electric aircraft, ensuring it stays within thermal limits.

Related literature: This study investigates two primary research areas. The first focuses on modeling electric vehicle power consumption, including battery system electrical and thermal modeling, and addressing thermal runaway behavior. Prior works have modeled ground vehicle battery systems at cell or system levels [5], [6] but lacked thermal conditioning to prevent overheating [7]. Modeling efforts for fully electric and hybrid-electric aircraft battery systems (BTMS) and thermal management have been limited. While some research emphasizes precise battery thermal estimation for mission planning [8], connections among individual cells are often overlooked, which limits the model fidelity. Other studies explore cooling technologies for hybrid-electric aircraft [9], [10], investigating factors influencing cooling

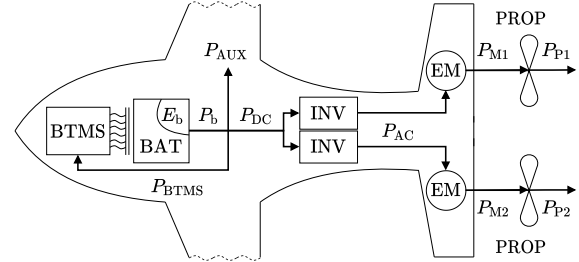


Fig. 1: Power block diagram showing the electric aircraft powertrain topology. It consists of a BTMS, a battery system (BAT), two inverters (INV), two electric motors (EM) and two propellers (PROP). The power flows (indicated by arrows), P_i , are battery output power, BTMS, inverter, and machine input power flows indicated with the subscripts for $i=\{b, \text{BTMS}, \text{DC}, \text{AC}\}$. Others are auxiliary loads, P_{aux} , and in-/output power to the propellers, P_M and P_P , respectively. The placement of some components in this schematic does not correspond to their actual location in the aircraft and is for visual convenience only.

performance and thermal runaway risk. Unlike hybrid-electric aircraft, where the battery system can be shut off during unsafe operation, fully electric aircraft lack this option, risking complete power loss. The second research area focuses on minimum-energy design for battery system thermal conditioning, using BTMS. Research in electronics often relies on forced air cooling at the module level, optimizing module spacing for efficient cooling [11]. Aviation-specific studies, such as for a 19-seater single-aisle hybrid-electric aircraft, have optimized BTMS design, assessing various heat pump technologies [12]. However, research for fully electric aircraft is lacking. Currently, no comprehensive studies address system design challenges for electric aviation at the battery system level, considering the impact of BTMS on flight range and energy consumption. Additionally, there is limited exploration of thermal runaway behavior in worst-case scenarios.

Statement of contributions: This work presents a mathematical framework that simulates the electrical power consumption of a compact 8-seater electric aircraft, with powertrain architecture shown in Fig. 1, across a predefined flight regime. The aircraft is equipped with high-specific energy density nickel manganese cobalt (NMC) Lithium-ion cells. Subsequently, it determines the heat generation of a pouch-type NMC battery system at cell level [13] to investigate if thermal management in the form of BTMS is needed. The framework then facilitates BTMS design optimization with a minimal-energy objective to keep the battery system within safe operation limits. Additionally, we define the thermal behavior of the cell under heating-induced thermal runaway (TR). Finally, we showcase our framework on a battery system design for an 8-seater fully electric lightweight aircraft, by determining theoretical flight range without BTMS and subsequently incorporating BTMS and minimizing the battery energy consumed over the flight regime.

The authors are with the Control Systems Technology (CST) section, Dep. of Mechanical Engineering, Eindhoven University of Technology (TU/e), Eindhoven, 5600 MB, The Netherlands, t.hofman@tue.nl

Organization: Section II presents the powertrain component modeling methods, the battery modeling approach and the BTMS modeling method for the aircraft design. It additionally introduces the thermal runaway modeling method and the minimum-energy-consumption design problem. Lastly, we discuss some limitations of this framework. In Section III, we showcase the framework for a fixed flight regime. Conclusions are drawn in Section IV, after which we provide an outlook on future research.

II. METHODOLOGY

This section presents the design optimization problem and its constraints that describe the electric aircraft powertrain, battery system and BTMS. We introduce the objective and aircraft powertrain component models, whereby we put particular emphasis on the battery model. Next, we extract the battery parameters from test data and introduce the thermal model for the battery system and BTMS. Subsequently, we introduce the battery thermal runaway model and summarize the problem. The aircraft powertrain we consider in this paper is shown in Fig. 1.

A. Objective

The objective in our optimization problem is to minimize the internal energy consumption of the battery over a fixed flight regime starting at $t = 0$ to the end time $t = t_f$, where t_f is the final time of the cycle. We define the internal battery energy consumption as

$$\min_p \Delta E_b(p), \quad (1)$$

where $\Delta E_b(p)$ is equal to the difference in internal battery energy as a function of p , which represents the set of design variables, $p = (T_{fl}, \dot{V}_{fl}, P_{BTMS, rated})$, being the temperature of the cooling fluid, the volumetric flow rate of the cooling fluid and the rated power of the BTMS, respectively. The state variable in this problem is battery energy $x(t) = E_b$. The difference of internal battery energy is defined by

$$\Delta E_b(p) = E_b(0) - E_b(t_f), \quad (2)$$

where $E_b(0)$ and $E_b(t_f)$ are the internal battery energy at the beginning and at the end of the flight regime, respectively.

B. Longitudinal Aircraft Dynamics

In this section, we model the aircraft as a longitudinal point mass with the required thrust output as a load on the electric motors using a quasi-static backward-facing modeling approach in the time domain. We consider a provided flight profile consisting of an exogenous speed trajectory $v(t)$ and height trajectory $h(t)$. Assuming that the pilot takes the actions necessary to follow the mission and that the mass of the aircraft remains constant over the flight cycle, the required thrust provided by the propellers is expressed by longitudinal point mass equation of motion as

$$F_T(t) = \frac{\frac{1}{2} \cdot \rho(h(t)) \cdot v^2(t) \cdot C_d \cdot S_w + m \cdot (g \cdot \sin(\gamma) + \dot{v}(t))}{\cos(\alpha)}, \quad (3)$$

where $\rho(h(t))$ is the air density as a function of aircraft height $h(t)$, $v(t)$ is the airspeed of the aircraft, C_d is the drag coefficient, S_w is the wing area, m is the mass of the aircraft g is Earth's gravitational constant, γ is the flight path angle and α is the angle of attack [14]. The applied coordinate system for the longitudinal aircraft dynamics is shown in Fig. 2. In this study, we define the total mass m of the aircraft as

$$m = m_{empty} + m_b + m_{BTMS}, \quad (4)$$

where m_{empty} is the total mass of the plane without the mass of the battery system, m_b , and mass of BTMS, m_{BTMS} .

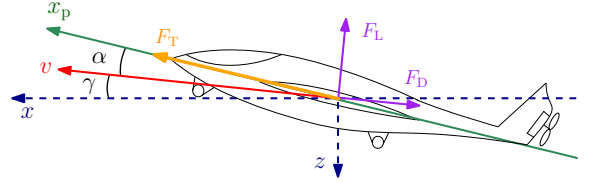


Fig. 2: Applied coordinate system for aircraft in flight for the use of a longitudinal point mass model, with components F_L and F_D , respectively, representing total lift and drag force. The flight path angle γ represents the direction of the flight, while the angle of attack α represents the angle of the wings w.r.t. the incoming air.

C. Powertrain model

In this study, we assume that both aircraft motors and both inverters perform identically over the flight cycle, thereby lumping them together to a single unit. For the motors, we consider axial flux permanent magnet synchronous machines (PMSM). To obtain the required electric motor power over the flight regime, we model a constant rotational speed, variable-pitch propeller connected to the motor shaft of both electric motors as a unified unit with

$$P_m(t) = \frac{F_T(t) \cdot v(t)}{\eta_p}, \quad (5)$$

where η_p is the propulsion efficiency of the propeller which accounts for the viscous profile drag on the blades, and for the kinetic energy lost in the accelerated airflow. Accordingly, the required motor torque is defined by

$$\tau_m(t) = \frac{P_m(t)}{\omega_m}, \quad (6)$$

where $\omega_m = \omega_{p, cons}$ is the rotational speed of the motor, which is equal to the propeller speed $\omega_{p, cons}$. From a modeling standpoint, the motor power is only limited by the maximum torque $\tau_{m, max}$ since the rotational speed is constant. Regeneration is not considered. The electrical power defined by the alternating current (AC) demanded at the inverter output is labeled $P_{AC}(t)$ and is expressed as

$$P_{AC}(t) = \frac{1}{\eta_m(\tau_m(t))} \cdot P_m(t), \quad (7)$$

where η_m is the motor efficiency as a function of motor torque for a constant rotational speed. The inverter provides power to the motor by rapidly alternating the direction of a direct current (DC) input, converting it into AC. Throughout this operation, there are experienced losses due to the rapid switching. We derive a quadratic model for these inverter losses, applying a general quadratic power loss model of the form

$$P_{DC}(t) = \beta \cdot P_{AC}^2(t) + P_{AC}(t), \quad (8)$$

where β is an efficiency parameter, subject to identification.

D. Battery model

The power at the battery system terminals is equal to the sum of all power consumers in the aircraft, defined by

$$P_b(t) = P_{DC}(t) + P_{BTMS}(t) + P_{aux}, \quad (9)$$

where $P_{BTMS}(t)$ represents the power drawn by the BTMS, and P_{aux} models a constant auxiliary power flow. In this context, the internal battery energy, E_b , changes with demanded internal battery power P_i as

$$\dot{E}_b(t) = -P_i(t), \quad (10)$$

where the minus sign ensures the battery is discharged when $P_b(t)$ is positive. Additionally, $E_b(t)$ is bounded by

$$E_b(t) \in [E_{b, min}, E_{b, max}], \quad (11)$$

where $E_{b, max}$ and $E_{b, min}$ correspond with the minimum and maximum battery state of charge levels, respectively, $\zeta_{b, min}$ and

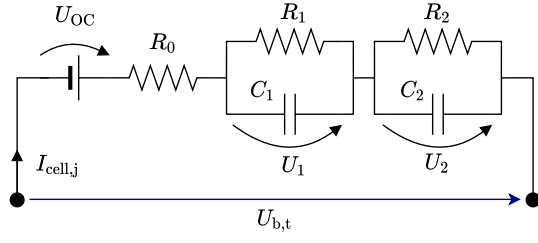


Fig. 3: Second-order equivalent circuit model diagram, consisting of an open-circuit voltage source U_{OC} , internal resistance R_0 and two RC pairs.

$\zeta_{b,max}$ by establishing the correlation between the variables in a lookup table. We assume the aircraft starts the flight regime with a fully charged battery

$$E_b(0) = \zeta_{b,max} \cdot E_{b,max}. \quad (12)$$

The internal battery power is defined as

$$P_i(t) = U_{OC}(\zeta(t)) \cdot I_b(t), \quad (13)$$

where U_{OC} is the open circuit voltage (OCV), defined by the cell's state of charge $\zeta(t)$. To obtain the battery current draw from the power demand, we apply

$$I_b(t) = \frac{P_b(t)}{n_s \cdot U_{cell,t}(t)}, \quad (14)$$

where n_s is the number of cells in series and $U_{cell,t}(t)$ is the battery cell's terminal voltage, which we obtain by applying an equivalent circuit model (ECM) with two RC-branches to provide a good trade-off between complexity and accuracy [15]. Fig. 3 illustrates this model, whereby component values vary with temperature and state of charge (SOC) [6]. The battery cell studied is an 11.84 Ah high specific energy density (HED) cell employing nickel manganese cobalt (NMC) chemistry, renowned for its balance of energy, power, cycle life, and thermal stability [16].

Next, we outline a single-cell modeling approach by a parallel circuit with n_p cells, employing an ECM featuring two RC elements. When n_p equals 1, the parallel circuit model transforms into that of a single cell. Therefore, by applying the total current draw defined in (14), we model the current draw $I_{cell,j}(t)$ of every cell $j \in \mathbb{N} \cap [1, n_p]$ in the parallel circuit as

$$I_{cell,j}(t) = \frac{I_b(t)}{n_p}. \quad (15)$$

Following the second-order ECM shown in Fig. 3, the terminal voltage of the cell under load is defined as

$$U_{cell,j}(t) = U_{OC}(\zeta(t)) - I_{cell,j}(t) \cdot R_0 - U_1(t) - U_2(t), \quad (16)$$

where R_0 is the cell's internal series resistance, $U_n(t)$ is the over-voltage over the n -th RC element, here with $n \in \{1, 2\}$.

We utilize the voltage and current data collected from the HPPC tests to fit the Equivalent Circuit Model (ECM) parameters with nonlinear regression utilizing a least-squares approach [17]. The result of HPPC data fit is shown in Fig. 4.

E. Battery thermal model

To minimize the workload in modeling and testing, LIBs are often treated as lumped thermal masses with consistent heat capacity. We assume uniform or piecewise uniform temperature distribution within the battery, enabling the feasibility of employing lumped elements for characterizing the battery's thermal dynamics. We can simplify the energy balance of every cell $j \in \mathbb{N} \cap [1, n_p]$ in the parallel circuit as

$$c_{p,j} \cdot m_{cell,j} \cdot \dot{T}_{cell,j}(t) = \dot{Q}_{gen,j}(t) + \dot{Q}_{diss,j}(t), \quad (17)$$

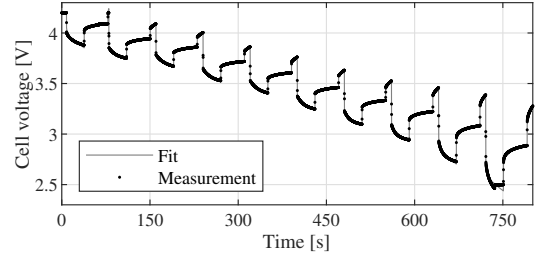


Fig. 4: Fit of HPPC cycle voltage for the 11.84 Ah NMC cell at 23 °C. The RMSE of the fit is 10.08 mV (0.58%).

where $c_{p,j}$ is the specific heat capacity of the cell, $m_{cell,j}$ is the mass of the cell, $T_{cell,j}(t)$ is the cell's temperature, $\dot{Q}_{gen,j}(t)$ is the cell's heat generation rate and $\dot{Q}_{diss,j}(t)$ is the heat dissipation rate. We consider both convective $\dot{Q}_{conv,j}(t)$ and radiative heat rate $\dot{Q}_{rad,j}(t)$, defined by

$$\dot{Q}_{diss,j}(t) = \dot{Q}_{conv,j}(t) + \dot{Q}_{rad,j}(t), \quad (18)$$

and

$$\dot{Q}_{conv,j}(t) = A \cdot h \cdot (T_{cell,j}(t) - T_{\infty,j}(t)), \quad (19)$$

where A is the cell's surface, h is the heat transfer coefficient, and T_{∞} is the environmental temperature around the cell, and with radiative heat rate defined by

$$\dot{Q}_{rad,j}(t) = A \cdot \varepsilon \cdot \sigma \cdot (T_{cell,j}^4(t) - T_{\infty,j}^4(t)), \quad (20)$$

where ε is the surface emissivity of the cell, taken as $\varepsilon = 0.8$ for this application and σ is the Stefan-Boltzmann constant ($\sigma = 5.67 \cdot 10^{-8} \text{ W} \cdot \text{m}^{-2} \cdot \text{K}^{-4}$). To model the heat generation rate $\dot{Q}_{gen,j}(t)$ of a battery on cell level, we apply an electric-thermal coupling model based on the assumption of uniform heat generation inside the battery cell proposed by Bernardi et al. [18]. The coupling model consists of two heat sources, $\dot{Q}_{irr,j}(t)$, the irreversible heat generated by the internal resistance of the cell and $\dot{Q}_{rev,j}(t)$, the reversible heat generation because of the entropy change due to the chemical reactions inside the cell. The heat generation rate can, therefore, be defined by

$$\dot{Q}_{gen,j}(t) = \dot{Q}_{irr,j}(t) + \dot{Q}_{rev,j}(t), \quad (21)$$

with

$$\dot{Q}_{irr,j}(t) = I_{cell,j}(t) \cdot (U_{OC}(\zeta(t)) - U_{cell,j}(t)), \quad (22)$$

and

$$\dot{Q}_{rev,j}(t) = I_{cell,j}(t) \cdot T_{cell,j}(t) \cdot \frac{\partial U_{OC}}{\partial T_{cell,j}}, \quad (23)$$

where $\frac{\partial U_{OC}}{\partial T_{cell,j}}$ is the entropy coefficient of the cell as introduced in [19]. For the cell-level simulation of a battery system comprising n cells, we omit consideration of thermal radiation as defined in (20). Consequently, temperatures may experience a slight overestimation, adding an inherent margin to the model.

F. Battery Thermal Management System model

A Battery Thermal Management System (BTMS) can be passive, using heat pipes and phase-change materials, or active, employing forced-air or liquid cooling systems [12]. Active systems utilize a liquid coolant to transfer heat from the battery to dissipation. Their effectiveness depends on factors such as fluid selection, mass flow, temperature control, and heat sink characteristics. In this study, we model an active BTMS incorporating a Vapor Cycle Machine (VCM), an established type of refrigeration system where a refrigerant undergoes phase changes to remove heat. The BTMS, comprising VCM, chiller, and coolant loop, is depicted in Fig. 5. We conceptualize the BTMS as a closed loop, where a fluid circulates through cooling channels integrated into aluminium cold plates. These cold plates

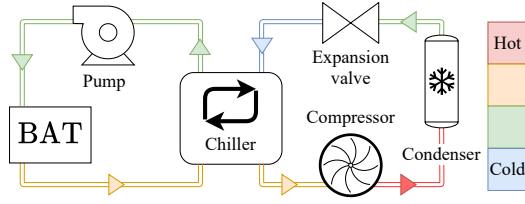


Fig. 5: BTMS system layout. Battery coolant loop left of the chiller, VCM on the right side. The actively controlled components are the pump and the compressor. The chiller represents a heat exchanger between the two loops.

function as heat sinks and are in direct physical contact with the battery cells. One of the main advantages of this BTMS layout is the high coefficient of performance, K_{BTMS} , depicting the ratio of useful heat energy produced to electrical energy consumption. The electrical power consumption of the BTMS, P_{BTMS} , influences the total electrical power consumption as stated in (9), which is modeled as

$$P_{BTMS}(t) = \frac{\dot{Q}_{BTMS}(t)}{K_{BTMS}}, \quad (24)$$

where $\dot{Q}_{BTMS}(t)$ is the heat dissipated by the fluid. As the mass and the electrical energy consumption of the BTMS both contribute to the total energy consumption of the aircraft, we express the mass of the BTMS as

$$m_{BTMS} = m_{loop} + m_{VCM}, \quad (25)$$

where m_{loop} and m_{VCM} represent the mass of the VCM and the mass of the coolant loop, respectively. The mass of the VCM is scaled with cooling power density ρ_P and defined as

$$m_{VCM} = \frac{P_{BTMS, rated}}{\rho_P}, \quad (26)$$

where $P_{BTMS, rated}$ is the rated cooling power of the BTMS and ρ_P is the specific power density of the VCM, expressed in cooling power per unit of mass. For electrical power, we need to divide this value by the coefficient of performance, K_{BTMS} .

The addition of a BTMS enables the system to dissipate heat via a cooling medium, thereby changing the dissipative properties of the environment around the cell, compared to purely natural heat dissipation. Therefore, we extend (18) to

$$\dot{Q}_{diss, j}(t) = \dot{Q}_{conv, j}(t) + \dot{Q}_{rad, j}(t) + \dot{Q}_{BTMS, j}(t), \quad (27)$$

with

$$\dot{Q}_{BTMS, j}(t) = A_{BTMS, j} \cdot h_{BTMS} \cdot (T_{cell, j}(t) - T_{fl, j}(t)), \quad (28)$$

where $A_{BTMS, j}$ represents the heat transferring area of the BTMS at cell j , h_{BTMS} denotes the mean heat transfer coefficient of the BTMS, and $T_{fl, j}$ signifies the inlet fluid temperature. We assume an isobaric, incompressible, and frictionless fluid within the BTMS. Flow through the BTMS is considered one-dimensional and strictly laminar. We employ the correlation for tube banks [20], ensuring conditions for cross- and longitudinal pitch ratios ($a < 1.2$, $b/a < 1.0$, and $Re < 10^4$). Here, a represents the transverse pitch ratio (s_t/D_h), b is the longitudinal pitch ratio (s_l/D_h), s_t is the transverse pitch, and s_l is the longitudinal pitch between channel centers. The channel, modeled as a plate duct, is formed by placing two plates at a fixed distance s_{ch} from each other. The mean convective heat transfer coefficient for the BTMS applied in (28) can be defined as

$$h_{BTMS} = \frac{k_{fl} \cdot \bar{Nu}}{D_h}, \quad (29)$$

where k_{fl} is the thermal conductivity of the fluid, $D_h = 2 \cdot s_{ch}$ the hydraulic diameter and \bar{Nu} is the mean Nusselt number. We apply approximate expressions defined for parallel plate ducts defined by Gnielinski [21] to reduce the complexity of the simulation. For strictly

laminar flow, the mean Nusselt number in parallel plate ducts is given by

$$\bar{Nu} = \sqrt[3]{Nu_1^3 + Nu_2^3}, \quad (30)$$

where $Nu_1 = 4.816$ for one heat-exchanging wall and

$$Nu_2 = 1.841 \cdot \sqrt[3]{Re \cdot Pr \cdot \frac{D_h}{l}}, \quad (31)$$

where Re is the Reynolds number, Pr is the Prandtl number ($Pr > 0.6$) [20] and l is the length of the cooling channel. The Reynolds number is equal to

$$Re = \frac{D_h \cdot v_{fl}}{\nu_{fl}}, \quad (32)$$

where v_{fl} is the velocity of the fluid, ρ_{fl} is the density of the fluid and ν_{fl} is the kinematic viscosity of the fluid. The velocity of the fluid is expressed as

$$v_{fl} = \frac{\dot{V}_{fl}}{A_{cross, ch}}, \quad (33)$$

where \dot{V}_{fl} is the volumetric flow rate of the cooling fluid and $A_{cross, ch}$ is the area of a channel's cross-section. The volumetric flow rate of the cooling fluid can be adjusted between zero and the maximum allowable flow rate for a certain channel size. As the fluid passes the cells within a cooling channel, it is heated up. Consequently, cells located at the outlet of the channel experience less cooling compared to those at the inlet.

G. Thermal runaway model

Understanding and predicting Thermal Runaway (TR) mechanisms is crucial for establishing early warning triggers in battery thermal management and devising effective prevention strategies. In this section, we adopt a simplified approach for modeling decomposition reactions proposed by [22], utilizing measurements from non-destructive accelerating rate calorimeter (ARC) tests. All decomposition reactions are grouped into a single global reaction for the cell [22], while Equations (17)-(20) are retained since the heat dissipation rate $\dot{Q}_{diss}(t)$ is independent of decomposition reactions. The generated heat flow $\dot{Q}_{gen}(t)$ describes the chemical reactions within the cell. For the thermal runaway scenario, we therefore redefine generated heat as

$$\dot{Q}_{gen, j}(t) = m_{cell} \cdot i_{react} \cdot \dot{x}_{cell}(t), \quad (34)$$

where i_{react} is the specific enthalpy of the cell reaction and $\dot{x}_{cell}(t)$ is the conversion reaction rate, expressed as

$$\dot{x}_{cell}(t) = A_x \cdot x_{cell} \cdot \exp\left(\frac{-E_A}{k_b \cdot T_{cell}}\right), \quad (35)$$

where A_x is the frequency factor, x_{cell} is the degree of conversion with $x_{cell} \in [0, 1]$, E_A is the activation energy of the reaction, and k_b is the Boltzmann constant ($k_b = 1.38 \cdot 10^{-23} \text{ J} \cdot \text{K}^{-1}$). We initiate the reaction at $x_{cell} = 1$, indicating that no reactant is consumed [23]. For the NMC type LIB applied in this study, the three values that characterize the overall chemical reaction of the cell, i_{react} , A_x and E_A , can be estimated from the cell temperature and temperature rate [24]. Since the validation of this model against real-world data requires destructive tests, we deem this validation to be beyond the scope of the current paper and devote it to future research.

H. Optimization problem

The objective is to minimize the battery energy consumption of the electric aircraft over a predefined flight regime. The capacity of its battery system $E_{b, max} = 304 \text{ kWh}$ is fixed as well, due to volume requirements. Therefore, we minimize the battery by finding the optimal BTMS size to retain sufficient cooling capacity and to avoid unnecessary weight increase. For this problem, the state variable are battery energy and cell temperature $x(t) = (E_b, T_{cell})$. The design

variables are $p = (T_{fl}, \dot{V}_{fl}, P_{BTMS, rated})$, being the temperature of the cooling fluid, the volumetric flow rate of the cooling fluid and the rated power of the BTMS, respectively.

Problem 1 (Nonlinear design problem). *The minimum energy design is the solution of*

$$\begin{aligned} \min_p \quad & \Delta E_b(p), \\ \text{s.t.} \quad & P_{b, \min} \leq P_b(t, p) \leq P_{b, \max}, \\ & U_{cell, \min} \leq U_{cell}(t, p) \leq U_{cell, \max}, \\ & T_{cell, opt, \min} \leq T_{cell}(t, p) \leq T_{cell, opt, \max}, \\ & E_b(t) \in [\zeta_{b, \min}, \zeta_{b, \max}] \cdot E_{b, \max}, \\ & 0 \leq I_b(t, p) \leq I_{b, \max}, \\ & P_{BTMS}(t, p) \leq P_{BTMS, rated}, \\ & \dot{V}_{fl, \min} \leq \dot{V}_{fl}(t) \leq \dot{V}_{fl, \max}, \\ & (2)-(16), (17)-(19), (21)-(23), (24)-(28). \end{aligned}$$

III. RESULTS

In this section, we present the battery system design as a result of the design constraints and requirements for the 8-seater light electric aircraft. Next, we present the numerical results of the optimal BTMS design. Lastly, we observe the TR behavior of the applied NMC cell.

A. Battery system design

Considering the constraints and framework outlined in Section II, we propose a baseline battery design for an 8-seater electric aircraft with a 304 kWh battery system, including BTMS. The design ensures failure redundancy by integrating two parallel individually switched battery banks, each at 400 V. These banks, connected to separate pairs of inverters and EMs, can be centrally controlled. The system features a 118-64 series-parallel cell layout to fit the aircraft's volume requirement. We analyze the theoretical flight range for an electric aircraft without BTMS, considering steady-state flight at 500 m and 180 km/h, discharging the battery from 100 to 15% SOC. The total system voltage constraint of 400 V requires the number of cells in series to remain constant. However, the number of parallel strings can vary. Fig. 6 illustrates this simulation across increasing parallel strings, affecting battery capacity and aircraft weight. The simulation considers multiple heat convection coefficients ($h = 0$ to $h = 7$), from no heat transfer to average convective heat transfer. The theoretical approach without convective heat transfer is impractical, with real-world scenarios always involving some form of heat transfer. Furthermore, it is observed that increasing parallel cells correlates with lower maximum cell temperatures. At $h = 7$, the temperature remains within the optimal range (28.5 °C). However, variations in heat convection levels throughout the flight cycle may push cells beyond this range. For instance, at $h = 3.5$, the temperature exceeds the optimal range (35.4 °C), jeopardizing operational safety. Additionally, increasing battery capacity could offer advantages, evident in the range curve's slight deflection tendency (Fig. 6).

B. Numerical results

We adopt a discrete-time approach, whereby we discretize the model using the trapezoidal method with a fixed step size of $\Delta t = 1$ s. We formulate the problem utilizing MATLAB and conduct the optimization by employing the nonlinear optimization solver `fmincon` for constrained problems. The aircraft is simulated over a flight cycle with a duration of 8000 s, a steady-state flight altitude of 500 m, shown in Fig. 7. Furthermore, we consider the aircraft,

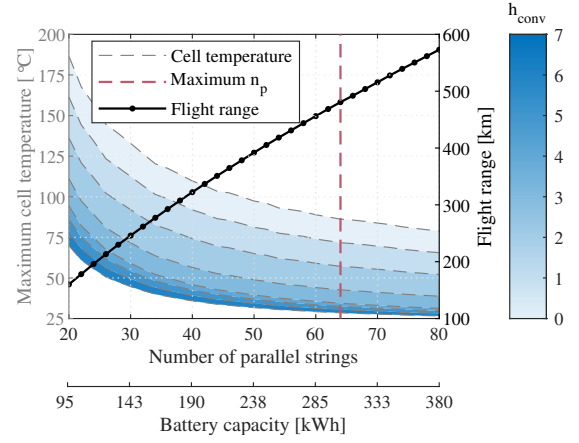


Fig. 6: Flight range and maximum cell temperature over the number of parallel battery strings, for varying heat transfer coefficient values h from 0 of 7 W/m²K. Steady-state flight at 500 m from 100-15% SOC and without BTMS added. Maximum parallel switched cell strings is 64 (red dotted line).

TABLE I: Numerical results for the minimum energy BTMS design. The theoretical range is calculated purely based on increased power consumption of the BTMS, disregarding temperature limits.

Cooling type	T_{fl} [°C]	\dot{V}_{fl} [m ³ /s]	P_{BTMS} [kW]	ΔE_b [kWh]	Aircraft weight [kg]	Theoretical flight range [km]
None	-	-	-	189.19	2345	480
Water	24.78	$3.96 \cdot 10^{-4}$	9.90	241.12	2732	410
Air		$6.5 \cdot 10^{-3}$				373

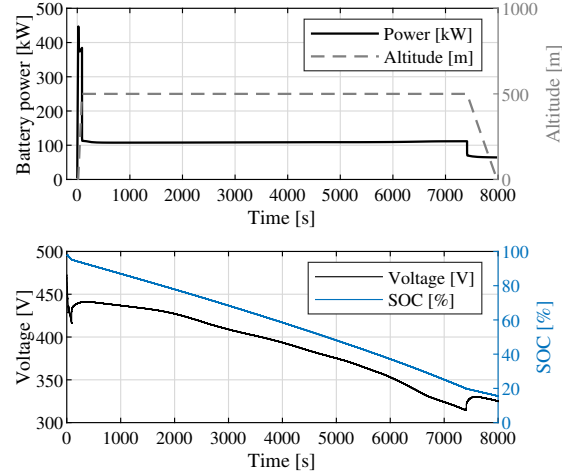


Fig. 7: Power demand of aircraft with water-cooled BTMS and flight altitude over time (top), voltage and SOC over flight regime (bottom).

battery system, and BTMS specifications of which the optimal design is obtained in the case of water and air cooling. The BTMS assumes a VCM with $K_{BTMS} = 3$ and $\rho_P = 100$ W/kg at an ambient temperature of 25 °C. Table I presents minimum energy consumption values for scenarios without BTMS, with water-cooled BTMS, and with air-cooled BTMS, along with corresponding optimal design variables (p). While air cooling achieves similar energy usage to water cooling, it fails to complete the cycle as a result of ineffective heat dissipation, as shown in Fig. 8. Water cooling maintains cells within their optimal

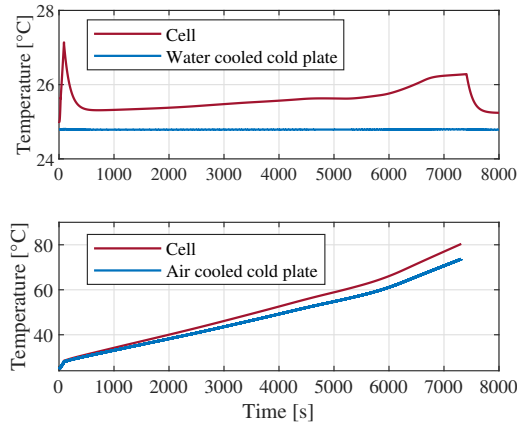


Fig. 8: Liquid cooling BTMS (top) and air cooling BTMS (bottom) over flight regime.

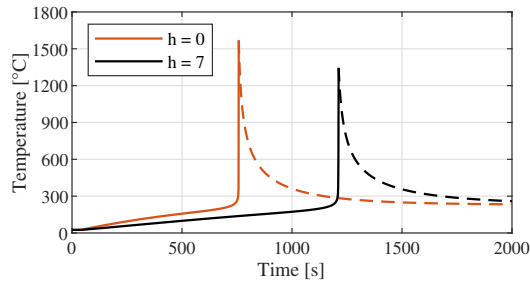


Fig. 9: TR predictions of cells for convective heat coefficients $h = 0 \text{ W/m}^2/\text{K}$ and $h = 7 \text{ W/m}^2/\text{K}$.

temperature range, as depicted in Fig. 7, adding 16.5% weight (387 kg) compared to no BTMS. Next, heating-induced thermal runaway is modeled separately at the cell level. An 11.84 Ah NMC cell is heated at a rate of $3^\circ\text{C}/\text{min}$, corresponding to full power demand. Simulation is conducted at two convection levels: none ($h = 0 \text{ W/m}^2/\text{K}$) and average ($h = 7 \text{ W/m}^2/\text{K}$). Fig. 9 illustrates cell temperature evolution, with TR trigger points at $t = 756 \text{ s}$ ($h = 0$) and $t = 1208 \text{ s}$ ($h = 7$). The critical ambient TR trigger temperature exceeds 182°C . In Fig. 6, even without BTMS and convection ($h = 0$), cell temperatures remain below 86°C throughout the flight, indicating no thermal runaway initiation.

IV. CONCLUSION

In this study, we proposed a system-level powertrain and battery sizing approach for light electric passenger aircraft, focusing on battery system design and safety. We developed a parametric framework simulating electrical power consumption across a predefined flight regime, considering thermal and electrical battery dynamics. Investigating the theoretical flight range without BTMS, we noted the impact of varying parallel strings on battery capacity and weight, finding range advantages with increased battery capacity up to the maximum aircraft weight. We proposed a VCM-based BTMS with bottom-mounted cold plates for water and air cooling to control the battery temperature, and its design to achieve minimum energy consumption. Our results showed inadequate heat dissipation and failure to complete the flight regime with air cooling due to constant full power draw, while water cooling meets operational constraints, adding 16.5% weight to the aircraft. The analysis of heating-induced thermal runaway demonstrated the effectiveness of the battery design in preventing thermal

runaway, even without BTMS and convection. Future research may focus on advancements in high-energy-density battery chemistries and integrating HVAC with BTMS to reduce power consumption.

ACKNOWLEDGMENT

We thank Dr. I. New for proofreading this paper. This paper was partly supported by the NEON research project (project number 17628 of the Crossover program which is (partly) financed by the Dutch Research Council (NWO)).

REFERENCES

- [1] B. A. Adu-Gyamfi and C. Good, "Electric aviation: A review of concepts and enabling technologies," 2022.
- [2] A. H. Epstein and S. M. O'Flarity, "Considerations for reducing aviation's CO2 with aircraft electric propulsion," *Journal of Propulsion and Power*, 2019.
- [3] G. L. Plett, *Battery Management Systems, Volume I: Battery Modeling*. Artech House, 2015.
- [4] S. Yang, S. Zhou, X. Zhou, F. Chen, Q. Li, Y. Lu, Y. Hua, and H. Deng, "Essential technologies on the direct cooling thermal management system for electric vehicles," 2021.
- [5] C. Reiter, L. Wildfeuer, N. Wassiliadis, T. Krah, J. Dimecker, and M. Lienkamp, "A holistic approach for simulation and evaluation of electrical and thermal loads in lithium-ion battery systems," in *2019 14th International Conference on Ecological Vehicles and Renewable Energies, EVER 2019*, 2019.
- [6] S. Wilkins, S. Van Sterkenburg, E. Hoedemaekers, B. Rosca, D. Danilov, and R. Baert, "Model identification for thermal modelling of a battery pack," in *EVS 2017 - 30th International Electric Vehicle Symposium and Exhibition*, 2017.
- [7] J. Schömann, "Hybrid-Electric Propulsion Systems for Small Unmanned Aircraft," TU München, Tech. Rep., 2012.
- [8] J. C. Chin, S. L. Schnulo, T. B. Miller, K. Prokopius, and J. Gray, "Battery performance modeling on maxwell x-57," in *AIAA Scitech 2019 Forum*, 2019.
- [9] R. Kabir, K. Kaddoura, F. P. McCluskey, and J. P. Kizito, "Investigation of a Cooling System for A Hybrid Airplane," in *2018 AIAA/IEEE Electric Aircraft Technologies Symposium, EATS 2018*, 2018.
- [10] J. M. Rheume and C. E. Lents, "Commercial hybrid electric aircraft thermal management system design, simulation, and operation improvements," in *AIAA Propulsion and Energy Forum and Exposition*, 2019, 2019.
- [11] K. Kirad and M. Chaudhari, "Design of cell spacing in lithium-ion battery module for improvement in cooling performance of the battery thermal management system," *Journal of Power Sources*, 2021.
- [12] H. Kellermann, S. Fuhrmann, M. Shamiyeh, and M. Hornung, "Design of a Battery Cooling System for Hybrid Electric Aircraft," *Journal of Propulsion and Power*, 2022.
- [13] I. Stefan, "High Energy Density Lithium-Ion Cells with Silicon Nanowire Anode Technology," Amprius Technologies, Inc., Fremont, CA, Tech. Rep., 2020.
- [14] M. V. Cook, *Flight Dynamics Principles*. Elsevier Ltd, 2007.
- [15] X. Hu, S. Li, and H. Peng, "A comparative study of equivalent circuit models for Li-ion batteries," *Journal of Power Sources*, 2012.
- [16] G. E. Blomgren, "The Development and Future of Lithium Ion Batteries," *Journal of The Electrochemical Society*, 2017.
- [17] M. K. Tran, A. Dacosta, A. Mevawalla, S. Panchal, and M. Fowler, "Comparative study of equivalent circuit models performance in four common lithium-ion batteries: LFP, NMC, LMO, NCA," *Batteries*, 2021.
- [18] D. Bernardi, E. Pawlikowski, and J. Newman, "General energy balance for battery systems," in *Electrochemical Society Extended Abstracts*, 1984.
- [19] A. Eddahech, O. Briat, and J. M. Vinassa, "Thermal characterization of a high-power lithium-ion battery: Potentiometric and calorimetric measurement of entropy changes," *Energy*, 2013.
- [20] F. P. Incropera, D. P. DeWitt, T. L. Bergman, and A. S. Lavine, *Fundamentals of Heat and Mass Transfer, Sixth Edition*. John Wiley & Sons, Inc., 2011.
- [21] V. Gnielinski, "G2 Heat Transfer in Concentric Annular and Parallel Plate Ducts," in *VDI Heat Atlas*. Springer, 2010.
- [22] I. Lalinde, A. Berrueta, P. Sanchis, and A. Ursúa, "Applied method to model the thermal runaway of lithium-ion batteries," in *21st IEEE International Conference on Environment and Electrical Engineering and 2021 5th IEEE Industrial and Commercial Power System Europe, IEEEIC / I and CPS Europe 2021 - Proceedings*, 2021.
- [23] A. Melcher, C. Ziebert, M. Rohde, and H. J. Seifert, "Modeling and simulation of the thermal runaway behavior of cylindrical Li-ion cells-computing of critical parameters," *Energies*, 2016.
- [24] S. Ohneseit, P. Finster, C. Floras, N. Lubenau, N. Uhlmann, H. J. Seifert, and C. Ziebert, "Thermal and Mechanical Safety Assessment of Type 21700 Lithium-Ion Batteries with NMC, NCA and LFP Cathodes—Investigation of Cell Abuse by Means of Accelerating Rate Calorimetry (ARC)," *Batteries*, 2023.